

PAPER

Photohole-oxidation-assisted anchoring of ultra-small Ru clusters onto TiO₂ with excellent catalytic activity and stability†

Cite this: *J. Mater. Chem. A*, 2013, **1**, 2461

Changming Li,^a Shitong Zhang,^a Bingsen Zhang,^b Dangsheng Su,^b Shan He,^a Yufei Zhao,^a Jie Liu,^a Fei Wang,^a Min Wei,^{*a} David G. Evans^a and Xue Duan^a

Ultra-small metal clusters with good activity and stability are of great significance for their practical applications in catalysis and materials science. Here we report a photohole-oxidation-assisted approach for anchoring ultra-small Ru clusters (~1.5 nm) with an extremely high density (~10¹⁷ m⁻²) onto TiO₂ support. The resulting clusters have good thermal stability and exhibit excellent long-term catalytic activity for the hydrogenation of CO₂ to methane (methanation). The anchoring process involves the oxidation of Ru³⁺ in solution by photogenerated holes on the TiO₂ surface to give tiny RuO₂ species (<0.8 nm) immobilized on the surface, followed by a H₂ reduction step to produce Ru⁰ clusters. Aberration-corrected high-resolution transmission electron microscopy (Cs-HRTEM) observations identify the Ru–Ru bond length contraction at the metal surface (relative to the interior of the particle) as well as bond length changes in the defect region at the metal–support interface. Density functional theory (DFT) calculations further demonstrate that the ultra-small Ru clusters are well stabilized and tightly anchored onto the TiO₂ substrate *via* Ru–O covalent bonding in the defect region of the metal–support interface. The high-dispersion of ultra-small Ru clusters as well as the strong chemical bonding at the interface account for their surprisingly high catalytic reactivity and excellent thermal/reaction stability. This synthetic method may open up a new way to fabricate thermally stable ultra-small metal clusters for practical industrial applications in catalysis.

Received 23rd November 2012
Accepted 18th December 2012

DOI: 10.1039/c2ta01205g

www.rsc.org/MaterialsA

1 Introduction

Small metal clusters exhibiting fascinating physical and chemical properties have recently attracted considerable attention for heterogeneous catalysis, owing to their amazingly high activity and/or selectivity.^{1–9} Although high catalytic activity can be exhibited by small clusters, their lack of stability is an inherent problem, especially for bare ultrafine metal clusters (with sizes below 2 nm), owing to the low thermal stability of metal nanoparticles¹⁰ and the harsh conditions required in most industrial catalytic processes. Therefore, there have been many attempts to develop routes to synthesize small metal clusters and stabilize the as-prepared clusters for the purpose of simultaneously achieving excellent catalytic activity and high stability for practical applications. For instance, several physical methods (*e.g.*, ALD,⁹ sputtering¹¹) and chemical approaches

including colloidal synthesis,^{12–16} *in situ* redox reactions¹⁷ or light-irradiation assisted photoreduction methods^{18–22} have been exploited to prepare small metal clusters; moreover, in order to protect these active clusters against sintering/aggregation under realistic reaction conditions, several methods (*e.g.*, physical barriers,²³ encapsulation,²⁴ formation of alloys^{25,26} or substrate effects^{27–29}) have also been employed. Despite all this progress, the fabrication of small pristine and clean metal clusters (below 2 nm) exhibiting high activity and stability simultaneously has rarely been reported and remains a challenging goal.

Ruthenium shows excellent activity in many industrially important catalytic processes, including ammonia synthesis and decomposition,^{30,31} selective oxidation³² and hydrogenation³³ reactions, and in particular is the best single metal catalyst for the hydrogenation of carbon dioxide.³⁴ Catalytic approaches for CO₂ fixation have attracted increasing interest in recent decades as a way to recycle CO₂ *via* its conversion into fuels (*e.g.*, methane).^{35,36} One of the major challenges for the practical application of this system is to develop efficient, economic and stable catalysts with high activity at relatively low temperature.^{11,35–39} This can be achieved by downsizing the Ru particles for more exposed active sites and anchoring them onto a suitable support to improve their stability.

^aState Key Laboratory of Chemical Resource Engineering, Beijing University of Chemical Technology, Beijing 100029, P. R. China. E-mail: weimin@mail.buct.edu.cn; Fax: +86 10-64425385; Tel: +86 10-64412131

^bShenyang National Laboratory of Materials Science, Institute of Metal Research, Chinese Academy of Sciences, Shenyang 110016, P. R. China

† Electronic supplementary information (ESI) available: Additional characterization results, density functional theory (DFT) calculations and further analysis. See DOI: 10.1039/c2ta01205g

Herein, we demonstrate the facile fabrication of ultra-small Ru clusters (~ 1.5 nm) on TiO_2 support with extremely high loading density ($\sim 10^{17}$ m^{-2}) as well as good thermal stability by using a photohole-oxidation-assisted method (denoted as Ru/ $\text{TiO}_2(\text{PO})$). The resulting material exhibits extraordinarily high activity and stability in the CO_2 methanation reaction, with a $>99\%$ conversion of CO_2 to CH_4 at a temperature as low as 220°C and long-term application without obvious activity loss. The high dispersion and superior stability of Ru clusters originate from the strong metal-support interaction observed by Cs-HRTEM; DFT calculations further reveal the formation of Ru-O chemical bonding in the defect region of metal-support interface, accounting for the excellent thermal/reaction stability of Ru/ $\text{TiO}_2(\text{PO})$. The generality of the photohole-oxidation method was also successfully demonstrated in the preparation of Ru/ CeO_2 or Fe/ TiO_2 systems. Our approach in this work holds significant promise for the design and fabrication of ultra-small metal clusters with both reactivity and stability for a variety of heterogeneous catalysis.

2 Experimental section

Materials

The TiO_2 (anatase, 25 nm), SiO_2 ($200\text{ m}^2\text{ g}^{-1}$) and $\text{RuCl}_3\cdot 3\text{H}_2\text{O}$ were purchased from Sigma-Aldrich. Deionized water was used in all the experimental processes.

Synthesis

The supported Ru/ $\text{TiO}_2(\text{PO})$ catalyst was prepared using a photohole-oxidation-assisted method. TiO_2 was dried at 120°C overnight and then suspended in an aqueous solution of RuCl_3 (80 mL, 7 mM) by ultrasonic treatment for 20 min. No organic sacrificial agent or surfactant was used. The resulting suspension was irradiated by ultraviolet light from a high-pressure Hg lamp (250 W) for 6 h with vigorous stirring. The solid was filtered using a high-speed centrifuge and washed thoroughly with deionized water. The resulting slurry was dried at 80°C for 24 h in a vacuum oven. The sample was subsequently reduced at 400°C for 3 h with a heating rate of 2°C min^{-1} in a hydrogen atmosphere. The Ru loading was 1.4 wt%, as determined by inductively coupled plasma-atomic emission spectroscopy (ICP-AES). To further be sure of the photohole-assisted oxidation process, a comparison deposition experiment was carried out under the same conditions except with the absence of UV-radiation.

For comparison, TiO_2 and SiO_2 supported Ru catalysts, denoted as Ru/ $\text{TiO}_2(\text{IMP})$ and Ru/ $\text{SiO}_2(\text{IMP})$ respectively, were prepared by the conventional impregnation method. The Ru loading of the two samples was also controlled to be 1.4 wt%. The samples were calcined in air at 400°C for 4 h and subsequently reduced by flowing H_2 at 400°C for 3 h.

Characterization

Hydrogen temperature programmed reduction (H_2 -TPR) and the hydrogen temperature programmed desorption (H_2 -TPD) were conducted in a quartz tube reactor on a Micromeritics

ChemiSorb 2720 with a thermal conductivity detector (TCD). In a typical H_2 -TPR process, 100 mg of a sample was sealed in the reactor, and then a gaseous mixture of H_2 and Ar (1 : 9, v/v) was fed to the reactor at 40 mL min^{-1} . The temperature was raised to 800°C at a heating rate of $10^\circ\text{C min}^{-1}$. For the H_2 -TPD process, 150 mg of a sample was first sealed and reduced in the reactor in the gaseous mixture of H_2 and Ar (1 : 9, v/v) at 400°C for 3 h. Subsequently, the reduced sample was purged in Ar at 450°C for 30 min, then cooled down to 25°C for readsorption of H_2 ; finally the temperature was raised to 800°C at a heating rate of $10^\circ\text{C min}^{-1}$ in Ar atmosphere. Powder XRD measurements were performed on a Rigaku XRD-6000 diffractometer, using Cu $K\alpha$ radiation ($\lambda = 0.15418\text{ nm}$) at 40 kV, 40 mA, with a scanning rate of 5° min^{-1} , and a 2θ angle ranging from 20° to 60° . A FEI Cs-corrected Titan 80-300 microscope operated at 300 kV was employed to conduct structural investigations of supported Ru samples by using TEM, HRTEM, and STEM modes. For the detection of the ultra-small Ru particles and estimation of the particle size distribution, high angle annular dark field imaging (HAADF) and elemental maps were used in the STEM mode. X-ray photoelectron spectra (XPS) were recorded on a Thermo VG Escalab 250 X-ray photoelectron spectrometer at a pressure of $\sim 2 \times 10^{-9}$ Pa with Al $K\alpha$ X-rays as the excitation source. The metal loading content in these supported Ru catalysts was determined by ICP-AES (Shimadzu ICPS-7500). The specific surface area measurements were performed based on Brunauer-Emmett-Teller (BET) method by using a Quantachrome Autosorb-1C-VP analyzer.

Catalytic tests

The activity tests of the supported Ru catalysts for CO_2 methanation were carried out in a quartz tube reactor (8 mm in diameter) at atmospheric pressure. Brooks mass flow controllers were used to control the gas flow rate. In order to eliminate temperature and concentration gradients, 0.5 g of the catalyst was mixed with 1.5 mL of inert quartz sand (40 to 60 mesh) and then packed into the reactor. The temperature of the reactor was controlled by three thermocouples (located near the entrance, at the middle, and near the exit of the bed). The catalyst bed length was 3.5 cm. After the catalyst pretreatment, the reaction gas mixture consisting of CO_2 and H_2 (1 : 4 molar ratio) was mixed with Ar (25%, v/v) at 60 standard cubic centimeters per minute (sccm) total flow rate was introduced into the reactor, and CO_2 conversion was measured over the temperature range 120 – 400°C . In each temperature, three hours or more time were needed until the conversion was steady. The product gas stream was analyzed on line by gas chromatography (GC, Shimadzu, 2014C) equipped with a thermal conductivity detector (TCD) and a flame ionization detector (FID). The condensate was also analyzed by gas chromatography-mass spectrometry (GC-MS) off-line. The CO_2 conversion and selectivity were calculated based on the CO_2 , H_2 and CH_4 mole fractions in the products. The turnover frequency (TOF) for CH_4 was calculated according to the metal dispersion estimated by H_2 -TPD results and the FID signal of CH_4 .

3 Computational methods

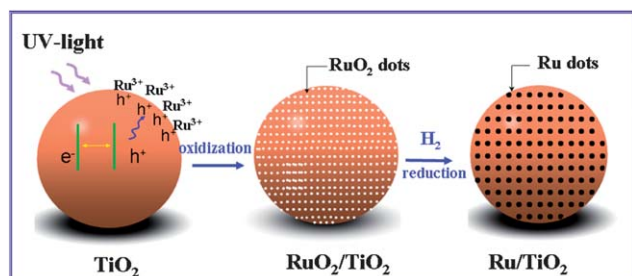
Periodic density functional theory (DFT) calculations were performed using the DMol3 code.⁴⁰ The (101) surface was simulated by a (3 × 4) slab (dimension size: 16.33 Å × 15.10 Å), with a thickness of four titanium layers. According to previously reported work, the (3 × 4) slab is large enough to reduce the interactions between neighboring images and allows the interfacial strain energy to be fully released.⁴¹ In addition, a vacuum space of 15.0 Å above the surface was employed to eliminate the interaction between two neighboring images along the vertical direction. All the atoms were fully relaxed during the geometric optimization. The generalized gradient approximation with the Perdew–Burke–Ernzerhof functional, together with effective core potentials was utilized. The basis set was specified as the double-numerical basis with polarization functions. The convergence criteria for structure optimizations were based on the following: (1) an energy tolerance of 2.0×10^{-5} Ha per atom; (2) a maximum force tolerance of 4.0×10^{-3} Ha Å⁻¹; (3) a maximum displacement tolerance of 4.0×10^{-3} Å. *k*-space was sampled by the gamma point. The metal–support interaction is described by the average adsorption energy, E_{ads} , which is defined by

$$E_{\text{ads}} = (nE(\text{Ru}) + E(\text{TiO}_2) - E(\text{Ru}/\text{TiO}_2))/n$$

where n is the total number of adsorbed Ru atoms; $E(\text{Ru})$, $E(\text{TiO}_2)$ and $E(\text{Ru}/\text{TiO}_2)$ are the total energy of individual Ru, the TiO₂ slab and the Ru/TiO₂ system.

4 Results and discussion

Although the photoreduction method has been widely used for the preparation of supported metal^{18–22,42} and metal oxide particles,^{43,44} the oxidative ability of photogenerated holes has been ignored and rarely explored to fabricate supported metal catalysts so far. Our strategy is schematically shown in Scheme 1. The fabrication process involves the oxidation of Ru³⁺ in solution by photogenerated holes on the TiO₂ surface to give immobilized tiny RuO₂ species, followed by a subsequent H₂ reduction step to produce ultra-small Ru⁰ clusters. In a typical photohole-oxidation-assisted immobilization process, TiO₂ nanocrystals (anatase) were suspended in a vigorously stirred aqueous solution of RuCl₃ under irradiation by UV light for 6 h



Scheme 1 Schematic illustration of the fabrication of supported ultra-small Ru clusters by the photohole-oxidation-assisted method.

(see details in the Experimental section). No organic sacrificial agent or surfactant was used, avoiding the possibility of introducing any impurities. X-ray photoelectron spectroscopy (XPS) studies on the resulting sample (denoted as RuO₂/TiO₂(PO)) showed two superimposed peaks at 280.6 and 281.5 eV (Fig. S1a†), which can be attributed to the Ru 3d_{5/2} bands of RuO₂ and hydrated RuO₂, respectively.⁴² The TEM image and EDS spectrum of the RuO₂/TiO₂(PO) material (Fig. S2†) also reveal the existence of supported tiny RuO₂ species with particle size less than 0.8 nm. The reactions/interactions of RuCl₃ with TiO₂ surface *via* OH groups and O-vacancies, *etc.*, are also possible for the support of Ru species on TiO₂ surface. However, the TEM image of the comparison sample without UV-radiation shows that a very small amount of Ru particles are supported on TiO₂ surface (Fig. S3†), in contrast to the highly dense immobilization by the photohole-assisted oxidation method (Fig. 1 and S2†). This indicates that Ru³⁺ in solution predominantly undergoes an oxidation reaction to form supported RuO₂ species by photogenerated holes^{42,45} under photoirradiation. Interestingly, the hydrogen temperature programmed reduction (H₂-TPR) curve of this material showed one main hydrogen consumption peak at a temperature of 450 °C (Fig. S4a†), which is significantly higher than the corresponding temperatures for a sample prepared by the conventional impregnation method (denoted as RuO₂/TiO₂(IMP), Fig. S4b†) or crystalline RuO₂ (Fig. S4c†). This indicates the presence of an enhanced interaction between the RuO₂ species and TiO₂ support in RuO₂/TiO₂(PO) relative to that in RuO₂/TiO₂(IMP).

After reduction of the RuO₂/TiO₂(PO) sample in H₂ at 400 °C for 3 h, the material gave a peak with a binding energy of 280.1 eV in its Ru 3d_{5/2} XPS spectrum (Fig. S1b†) which confirms the

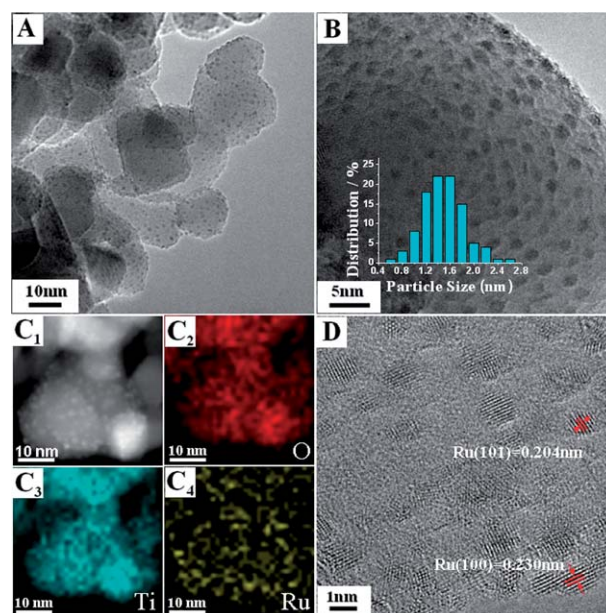


Fig. 1 Electron microscopy images of Ru/TiO₂(PO): TEM images with (A) low and (B) high magnification with size-distribution shown in the inset (300 Ru particles analyzed); (C₁) scanning transmission electron microscope (STEM) image of Ru/TiO₂(PO) and the elemental mapping images of: (C₂) O, (C₃) Ti, (C₄) Ru; (D) HRTEM image of the supported Ru clusters.

formation of Ru^0 species ($\text{Ru}/\text{TiO}_2(\text{PO})$). No characteristic reflections of Ru metal were observed in the XRD pattern (Fig. S5b[†]) however, indicative of the small size of the resulting Ru particles. A TEM image reveals that small Ru clusters are highly dispersed throughout the TiO_2 support (Fig. 1A); a homogeneous and uniform immobilization of Ru particles was observed with an average diameter of 1.5 ± 0.3 nm (Fig. 1B). High-angle annular dark field micrographs (HAADF-STEM) and the corresponding energy-dispersive spectroscopy (EDS) analysis further confirm the uniform dispersion of Ru clusters on the support (Fig. 1C). The loading density of the supported Ru clusters was calculated to be $\sim 10^{17} \text{ m}^{-2}$ according to the electron microscopy image, which is an order of magnitude or more higher than those for supported metal catalysts reported previously.⁴⁶ A high-resolution TEM image (Fig. 1D) reveals the single crystalline nature of the Ru clusters. The fringes with lattice spacings of 0.204 and 0.230 nm can be indexed to the (101) and (100) plane of hexagonal close-packed (hcp) Ru. It is worth noting that no obvious agglomeration occurs for the supported ultra-small Ru clusters even when calcined at temperatures up to 600 °C in a reducing atmosphere (Fig. S6[†]), indicating their exceptional thermal stability. A combination of such uniform dispersion of ultra-small Ru clusters with extraordinarily high loading density and excellent thermal stability has not been previously reported. Moreover, the generality of this method was also successfully demonstrated in the preparation of Ru/CeO_2 and Fe/TiO_2 systems (Fig. S7[†]).

The aberration-corrected high-resolution transmission electron microscopy (Cs-HRTEM) technique was employed to reveal the detailed fine atomic structure of the ultra-small Ru clusters supported on TiO_2 . Fig. 2 displays an atom-resolved HRTEM image of a representative Ru cluster with the [111] zone axis parallel to the primary electron beam. The lattice fringes (110), (10 $\bar{1}$) and (0 $\bar{1}$ 1) of Ru with mutual angles of 63.9° and 52° were identified for a typical Ru particle based on the PDF card (no. 06-0663) with space group $P63/mmc$. In this orientation, atomic columns are expected to be aligned within the (1 $\bar{1}$ 0) plane, (10 $\bar{1}$) plane and the equivalent (0 $\bar{1}$ 1) plane. On the basis of this

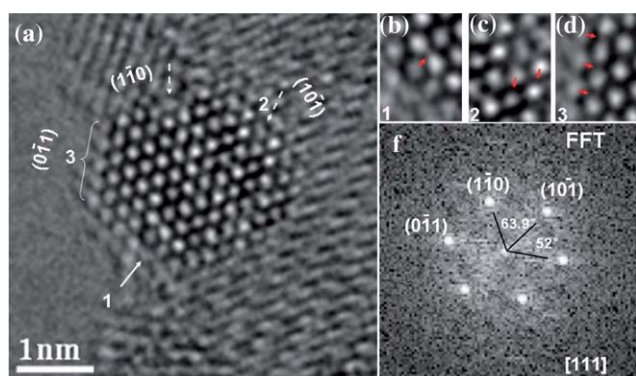


Fig. 2 Typical atom-resolved HRTEM image of a representative ultra-small Ru cluster (a), exhibiting monatomic surface steps (solid arrows), atomic vacancies (dashed arrows), and surface contraction (curly braces); the corresponding atomic displacements of these surface sites (b), (c) and (d); the local Fast Fourier Transform (FFT) of the HRTEM image (f).

information and the observed angles between the terminating planes, the exposed facets of the projected particle can be identified as mainly the low-index planes such as (100), (101) and (002). Monatomic surface steps and atomic vacancies are also detected at the surface of these low-index planes. Interestingly, based on the intercolumn distance analysis (Fig. S8[†]), a contraction of 0.2–0.6 Å for the surface Ru–Ru bond length relative to the bulk phase is observed at surface defect sites (steps and vacancies) (Fig. 2b and c) or at the outermost surface atoms (Fig. 2d), as denoted by the red arrows. The bond length contraction of the surface relative to the interior is a basic and important structural property of free nanocrystal surfaces. In this work, the bond length contraction directly observed by Cs-HRTEM on surface of the ultra-small Ru cluster can be attributed to the smoothing of surface electron density and the resulting electrostatic force that pulls the surface atoms towards the bulk, or to a change in chemical bonding where a decrease in coordination number strengthens the remaining bonds.⁴⁷ The bond length contraction is believed to play an important role in interfacial stability and the resulting catalytic behavior, as will be discussed in the following section.

Direct atom-resolved observation from the direction parallel to the contact plane between the metal and support, so-called “profile imaging” in TEM, can provide crucial structural information about metal–oxide interactions at the atomic scale.^{48,49} Fig. 3 displays a typical HRTEM image of the interfaces between Ru nanocrystals and TiO_2 recorded under profile view conditions. For TiO_2 (anatase), the (101) lattice spacing of 0.350 nm is readily observed. The protruding tiny particles at the edges of the TiO_2 were identified as small Ru nanocrystals according to the lattice fringes observed. The hemispherical/oblate shapes of the Ru nanoclusters are clearly seen in this magnified profile image, with a width–height ratio >2 and a small contact angle of less than 90° on TiO_2 (Fig. 3, inset). Hemispherical/oblate Ru nanoparticles with such a small size cannot be stabilized without a significant metal–support interaction. Indeed, structural distortions and poorly resolved lattice fringes with high defect concentration at metal–support interfaces are observed (Fig. 3, dashed green arrows), further confirming that a strong interaction is present at the interface between Ru nanoclusters and the support. Further evidence for this was provided by the

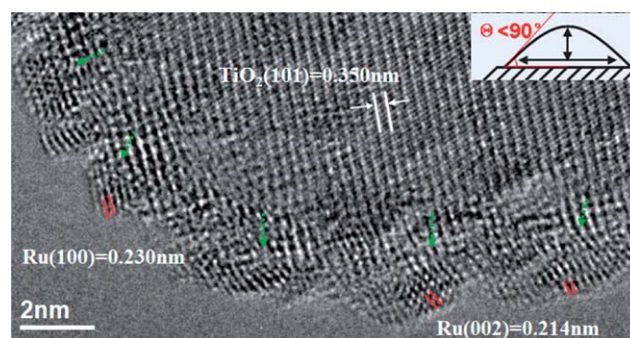


Fig. 3 Atomic-resolution cross-sectional HRTEM image of the interface between ultra-small Ru clusters and TiO_2 with the morphology model shown in the inset. The defect region is clearly observed at the interface (shown by the green arrows).

comparison of Ru 3d_{5/2} XPS spectrum between Ru/TiO₂(PO) (Fig. S1b†) and Ru/TiO₂(IMP) sample (Fig. S1c†). A broad peak which consists of 280.0 eV (Ru 3d_{5/2} of metallic Ru) and 280.8 eV (Ru 3d_{5/2} of Ru^{δ+}) was observed for the Ru/TiO₂(PO) sample, indicating some degree of oxidation of Ru clusters to Ru^{δ+} species. In addition, the Ti 2p peak undergoes a negative shift (~0.18 eV) in the Ru/TiO₂(PO) sample relative to pristine TiO₂ (Fig. S9†), implying partial reduction of the TiO₂ substrate. This is probably due to the sharing of O atoms at the defect region of interface.^{50,51} Owing to the rich unsaturated coordination atoms and high energy state of small Ru clusters, the metal–support interaction is expected to reduce both the unsaturated bonds and the high surface energy of metal clusters.

To obtain further insight into the interfacial interaction between Ru and TiO₂ at the atomic scale, density functional theory (DFT) calculations were carried out to simulate the nucleation and growth of Ru clusters by using Ru_{*n*} (*n* = 1–4) cluster models on anatase TiO₂(101) (Fig. 4; see details in the ESI†). It was found that the O atoms neighboring Ru clusters moved from their equilibrium positions towards the highly unsaturated Ru atoms, with the formation of Ru–O bonds resulting in the weakening of the Ti–O bonds. Furthermore, with increasing value of *n*, both the Ru–O bond length and the average adsorption energy gradually decreased, which indicates that the migration of O towards Ru reduces the Ru interaction with the neighboring Ru atoms. Accordingly, it can be proposed that the establishment of the Ru–O interaction leads to the disturbance of both Ti–O and Ru–Ru bonds, in accordance with

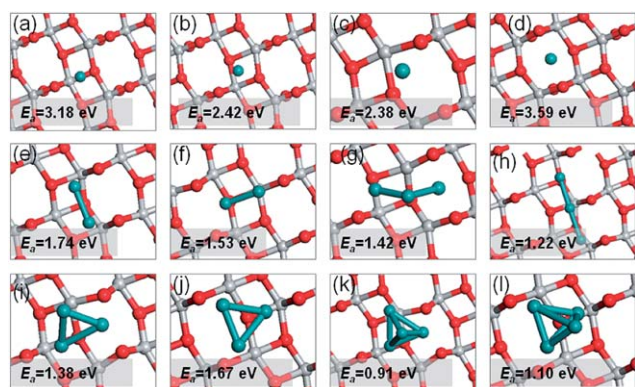


Fig. 4 DFT calculations of the optimized geometries of Ru_{*n*} (*n* = 1–4) on a TiO₂(101) surface with various adsorption energies. For the sake of clarity, only atoms in the first layer are shown (Ti, grey; O, red; Ru, green).

the distorted and poorly resolved lattice fringes at the metal–support interface observed by Cs-HRTEM. To further understand the electronic interaction between Ru_{*n*} and the TiO₂ support, the total and local densities of states (TDOS and LDOS) as well as the electron densities for a clean TiO₂(101) surface and the Ru_{*n*}/TiO₂ systems were calculated (Fig. S10 and S11†). The results show a high electron delocalization between coupled Ru and O atoms, further indicating that the interface is predominantly composed of Ru–O bonds. No evidence for metallic Ti–Ru bonding was observed. Taken together with the Cs-HRTEM and XPS results, the DFT calculations demonstrate the ultra-small Ru clusters are well stabilized and tightly anchored onto the TiO₂ substrate *via* Ru–O covalent bonding at the defect region of the interface.

The catalytic performance of Ru/TiO₂(PO) was evaluated using CO₂ methanation as a probe reaction, and compared with the performances of Ru/TiO₂(IMP) and Ru/SiO₂(IMP) with the same Ru loadings prepared by a conventional impregnation method. The detailed information for these catalysts is summarized in Table 1. The mean Ru particle sizes of 5.2 ± 0.5 nm and 9.1 ± 0.8 nm (Fig. S12†), respectively, in these comparison materials were significantly larger than that in Ru/TiO₂(PO) (1.5 ± 0.3 nm). Fig. 5A shows the yield of CH₄ as a function of reaction temperature for the three samples. The supported ultra-small Ru cluster catalyst (Ru/TiO₂(PO)) exhibits an extraordinarily high activity with a >99% conversion of CO₂ to CH₄ at a temperature as low as 220 °C, which is significantly better than the performance of either Ru/TiO₂(IMP) or Ru/SiO₂(IMP). The hydrogen temperature programmed desorption (TPD) measurements were also carried out to estimate the metal dispersion of these catalysts, and the turnover frequency (TOF)

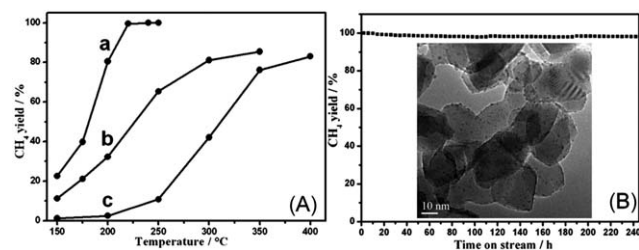


Fig. 5 (A) Temperature dependence of the yield of methane for CO₂ methanation over supported Ru catalysts: (a) Ru/TiO₂(PO), (b) Ru/TiO₂(IMP), (c) Ru/SiO₂(IMP); (B) time-on-stream analysis for Ru/TiO₂(PO) at 220 °C (the inset shows the TEM image of Ru/TiO₂(PO) catalyst after the CO₂ methanation reaction for 240 h).

Table 1 Structural characterization and CO₂ methanation activity for various catalysts

Sample	Ru content/wt%	Specific surface area/m ² g ⁻¹	Metal dispersion (<i>D</i>) by H ₂ -TPD ^a	Mean particle size by H ₂ -TPD ^a /nm	Mean particle size by TEM/nm	TOF ^b of CH ₄ at 120 °C/s ⁻¹
Ru/TiO ₂ (PO)	1.4	52	0.69	1.3	1.5 ± 0.3	1.04 × 10 ⁻³
Ru/TiO ₂ (IMP)	1.4	46	0.19	4.8	5.2 ± 0.5	3.46 × 10 ⁻⁴
Ru/SiO ₂ (IMP)	1.4	256	0.09	9.6	9.1 ± 0.8	4.40 × 10 ⁻⁵

^a The metal dispersion and particle size were obtained from the H₂-TPD results.⁵² ^b The TOF value was calculated based on the metal dispersion measured by H₂-TPD and the yield of CH₄ at 120 °C.

for CH₄ at 120 °C was calculated based on the TPD results (Fig. S13[†], Table 1). The Ru/TiO₂(PO) sample exhibits the highest metal dispersion ($D = 0.69$) as expected, and the mean size of Ru clusters estimated by the TPD data is close to the TEM observation. The TOF value of Ru/TiO₂(PO) catalyst is 1.04×10^{-3} , three and twenty times higher than that of Ru/TiO₂(IMP) (3.46×10^{-4}) and Ru/SiO₂(IMP) (4.40×10^{-5}), respectively, further indicating the highest activity of Ru/TiO₂(PO) catalyst towards CO₂ methanation at low temperature. In addition, neither obvious decrease in the catalytic activity of Ru/TiO₂(PO) (Fig. 5B) nor significant sintering (Fig. 5B, inset) was observed after reaction for ten days (240 h), indicating sufficient stability for long-term employment even in the case of a strongly exothermic reaction such as CO₂ methanation ($\Delta H_{298\text{K}} = -252.9 \text{ kJ mol}^{-1}$). The ultra-small particle size and high density of the supported Ru clusters facilitate a sufficient exposure of the low-coordination, unsaturated metal surface sites observed by Cs-HRTEM, accounting for the high activity of Ru/TiO₂(PO) at low temperature. Moreover, the anchoring effect resulting from the strong covalent bonding in the defect region of the metal-support interface revealed by DFT calculations is responsible for the satisfactory reaction stability of the Ru clusters with respect to migration or sintering. The results conclusively demonstrate that the highly dispersed and stable Ru/TiO₂(PO) material can serve as an efficient catalyst for the CO₂ methanation reaction.

5 Conclusion

In summary, we have developed a facile methodology for the preparation of supported ultra-small Ru clusters with high-density, excellent catalytic activity and good thermal/reaction stability, by using the photohole-oxidation-assisted immobilization of tiny RuO₂ species (<0.8 nm) onto TiO₂ support followed by a subsequent reduction process. Cs-HRTEM studies of the resulting Ru/TiO₂(PO) material give direct evidence for both the bond length changes at the metal surface and in the defect region at the metal-support interface. DFT calculations further reveal the formation of Ru–O bonds as well as the weakening of Ti–O bonding and the decreased average adsorption energy, in accordance with the experimental results. The high dispersion of ultra-small Ru clusters as well as the strong covalent bonding at the interface account for the observed surprisingly high reactivity and good thermal/reaction stability of the Ru/TiO₂(PO) catalyst. This work not only provides a facile method for the preparation of highly dispersed ultra-small Ru clusters serving as an excellent methanation catalyst, but also offers a fundamental understanding of the influence of chemical bonding on structure–function correlations. It is expected that this strategy can be extended to the fabrication of other supported metal nanoclusters with significantly enhanced activity and long-term stability in heterogeneous catalysis.

Acknowledgements

This work was supported by the 973 Program (Grant no. 2011CBA00504) and the National Natural Science Foundation of

China (NSFC). M. Wei particularly appreciates the financial aid from the China National Funds for Distinguished Young Scientists of the NSFC.

Notes and references

- 1 A. T. Bell, *Science*, 2003, **299**, 1688.
- 2 R. Schlögl and S. B. A. Hamid, *Angew. Chem., Int. Ed.*, 2004, **43**, 1628.
- 3 J. Hutchings, M. Brust and H. Schmidbaur, *Chem. Soc. Rev.*, 2008, **37**, 1759.
- 4 U. Heiz and E. L. Bullock, *J. Mater. Chem.*, 2004, **14**, 564.
- 5 Q. Wang and D. O'Hare, *Chem. Rev.*, 2012, **112**, 4124.
- 6 A. A. Herzing, C. J. Kiely, A. F. Carley, P. Landon and G. J. Hutchings, *Science*, 2008, **321**, 1331.
- 7 S. H. Mushrif, A. D. Rey and G. H. Peslherbe, *J. Mater. Chem.*, 2010, **20**, 60.
- 8 B. T. Qiao, A. Q. Wang, X. F. Yang, L. F. Allard, Z. Jiang, Y. T. Cui, J. Y. Liu, J. Li and T. Zhang, *Nat. Chem.*, 2011, **3**, 634.
- 9 S. Vajda, M. J. Pellin, J. P. Greeley, C. L. Marshall, L. A. Curtiss, G. A. Ballentine, J. W. Elam, S. Catillon-Mucherie, P. C. Redfern, F. Mehmood and P. Zapol, *Nat. Mater.*, 2009, **8**, 213.
- 10 Ph. Buffat and J.-P. Borel, *Phys. Rev. A*, 1976, **13**, 2287.
- 11 T. Abe, M. Tanizawa, K. Watanabe and A. Taguchi, *Energy Environ. Sci.*, 2009, **2**, 315.
- 12 A. Roucoux, J. Schulz and H. Patin, *Chem. Rev.*, 2002, **102**, 3757.
- 13 N. Perkas, Z. Y. Zhong, L. W. Chen, M. Besson and A. Gedanken, *Catal. Lett.*, 2005, **103**, 9.
- 14 N. F. Zheng and G. D. Stucky, *J. Am. Chem. Soc.*, 2006, **128**, 14278.
- 15 S. Chen, D. A. Maclaren, R. T. Baker, J. N. Chapman, S. Lee, D. J. Cole-Hamilton and P. Andre, *J. Mater. Chem.*, 2011, **21**, 3646.
- 16 M. Aslam, L. Fu, M. Su, K. Vijayamohan and V. P. Dravid, *J. Mater. Chem.*, 2004, **14**, 1795.
- 17 G. C. Xi, G. H. Ye, Q. Ma, L. Su, H. Bai and C. Wang, *J. Am. Chem. Soc.*, 2012, **134**, 6508.
- 18 J. Ohyama, A. Yamamoto, K. Teramura, T. Shishido and T. Tanaka, *ACS Catal.*, 2011, **1**, 181.
- 19 S. F. Chen, J. P. Li, K. Qian, W. P. Xu, Y. Lu, W. X. Huang and S. H. Yu, *Nano Res.*, 2010, **3**, 244.
- 20 K. Teramura, S. I. Okuoka, S. Yamazoe, K. Kato, T. Shishido and T. Tanaka, *J. Phys. Chem. C*, 2008, **112**, 8495.
- 21 A. Fernandez, A. Caballero and A. R. Gonzalez-Elipe, *J. Phys. Chem.*, 1995, **99**, 3303.
- 22 B. Kraeutler and A. J. Bard, *J. Am. Chem. Soc.*, 1978, **100**, 4317.
- 23 F. Tang, N. Ma, X. Y. Wang, F. He and L. D. Li, *J. Mater. Chem.*, 2011, **21**, 16943.
- 24 Y. Wang, A. S. Angelatos and F. Caruso, *Chem. Mater.*, 2008, **20**, 848.
- 25 A. Cao and G. Veser, *Nat. Mater.*, 2010, **9**, 75.
- 26 Y. Ding, F. Fan, Z. Q. Tian and Z. L. Wang, *J. Am. Chem. Soc.*, 2010, **132**, 12480.

- 27 M. Q. Zhao, Q. Zhang, W. Zhang, G. Q. Huang, Y. H. Zhang, D. S. Su and F. Wei, *J. Am. Chem. Soc.*, 2010, **132**, 14739.
- 28 M. Q. Zhao, Q. Zhang, J. Q. Huang and F. Wei, *Adv. Funct. Mater.*, 2012, **22**, 675.
- 29 W. F. Yan, S. Brown, Z. W. Pan, S. M. Mahurin, S. H. Overbury and S. Dai, *Angew. Chem., Int. Ed.*, 2006, **45**, 3614.
- 30 Z. Song, T. H. Cai, J. C. Hanson, J. A. Rodriguez and J. Hrbek, *J. Am. Chem. Soc.*, 2004, **126**, 8576.
- 31 A. M. Karim, V. Prasad, G. Mpourmpakis, W. W. Lonergan, A. L. Frenkel, J. G. Chen and D. G. Vlachos, *J. Am. Chem. Soc.*, 2009, **131**, 12230.
- 32 X. M. Yang, X. N. Wang and J. S. Qiu, *Appl. Catal., A*, 2010, **382**, 131.
- 33 Z. Y. Sun, Z. M. Liu, B. X. Han, Y. Wang, J. M. Du, Z. L. Xie and G. J. Han, *Adv. Mater.*, 2005, **17**, 928.
- 34 G. A. Mills and F. W. Steffgen, *Catal. Rev.*, 1973, **8**, 159.
- 35 W. Wang, S. P. Wang, X. P. Ma and J. L. Gong, *Chem. Soc. Rev.*, 2011, **40**, 3703.
- 36 Y. Zhu, S. R. Zhang, Y. C. Ye, X. Q. Zhang, L. Wang, W. Zhu, F. Cheng and F. Tao, *ACS Catal.*, 2012, **2**, 2403.
- 37 S. Sharma, Z. P. Hu, P. Zhang, E. W. McFarland and H. Metiu, *J. Catal.*, 2011, **278**, 297.
- 38 F. Ocampo, B. Louis and A.-C. Roger, *Appl. Catal., A*, 2009, **369**, 90.
- 39 F. Ocampo, B. Louis, L. Kiwi-Minsker and A.-C. Roger, *Appl. Catal., A*, 2011, **392**, 36.
- 40 B. Delley, *J. Chem. Phys.*, 1990, **92**, 508.
- 41 C. H. Sun and S. C. Smith, *J. Phys. Chem. C*, 2012, **116**, 3524.
- 42 T. Kobayashi, Y. Taniguchi, Y. Yoneyama and H. Tamura, *J. Phys. Chem.*, 1983, **87**, 768.
- 43 A. Mills, P. A. Duckmanton and J. Reglinski, *Chem. Commun.*, 2010, **46**, 2397.
- 44 K. Maeda, K. Teramura, D. Lu, N. Saito, Y. Inoue and K. Domen, *Angew. Chem., Int. Ed.*, 2006, **118**, 7906.
- 45 A. J. Bard, *Science*, 1980, **207**, 139.
- 46 R. Zanella, S. Giorgio, C. R. Henry and G. Louis, *J. Phys. Chem. B*, 2002, **106**, 7634.
- 47 W. J. Huang, R. Sun, J. L. Tao, D. Menard, R. G. Nuzzo and J. M. Zuo, *Nat. Mater.*, 2008, **7**, 308.
- 48 N. Shibata, A. Goto, S. Y. Choi, T. Mizoguchi, S. D. Findlay, T. Yamamoto and Y. Ikuhara, *Science*, 2008, **322**, 570.
- 49 F. R. Fan, Y. Ding, D. Y. Liu, Z. Q. Tian and Z. L. Wang, *J. Am. Chem. Soc.*, 2009, **131**, 12036.
- 50 H. Hata, Y. Kobayashi, V. Bojan, W. J. Youngblood and T. E. Mallouk, *Nano Lett.*, 2008, **8**, 794.
- 51 U. Diebold, *Surf. Sci. Rep.*, 2003, **48**, 53.
- 52 X. F. Shen, L.-J. Garces, Y. S. Ding, K. Laubernds, R. P. Zenger, M. Aindow, E. J. Neth and S. L. Suib, *Appl. Catal., A*, 2008, **335**, 187.